ELSEVIER

Journal of Alloys and Compounds 300–301 (2000) 71–87

Journal of ALLOYS AND COMPOUNDS

www.elsevier.com/locate/jallcom

Spectroscopy and structure of selected lanthanide polymeric and monomeric systems

Janina Legendziewicz*

University of Wrocław, Faculty of Chemistry, 14 F. Joliot-Curie Str., 50-383 Wrocław, Poland

Abstract

In recent years many studies have been devoted to polynuclear compounds because of their unusual structural features and/or magnetic and optical properties. This lecture deals with a group of homo- and heteronuclear polymeric, as well as monomeric, lanthanide systems. It will be shown that several structural factors influence in a special way their spectroscopic and magnetic properties. Absorption, emission and excitation spectra down to 5 K will be analysed and related to X-ray crystallographic data. Radiative and non-radiative processes will be considered; cooperative interactions and the role of vibronic coupling, including the resonance effect, will be analysed. Spectroscopic properties of the complexes will be correlated with magnetic and EPR data. Selected dynamics aspects in the solid state will also be discussed.

Keywords: Lanthanide; Polymeric and monomeric systems; X-Ray crystallography; Spectroscopy; Cooperative interactions; Vibronic coupling

1. Introduction

In last two decades increased interest has been observed in the study of lanthanide dimer and polymer systems. This has mainly been motivated by the development of infrared-to-visible up-conversion laser materials, and by observations and investigations of cooperative processes in biological systems. In this paper the main attention is focused on the structure of this new class of lanthanide compounds, their electron spectroscopy; and radiative and non-radiative processes. Several new developments are included arising from investigations of cooperative ion-pair (d and f) interactions leading to certain important optical and magnetic properties. Selected aspects of these studies will be presented and discussed on the basis of the results obtained for three classes of these compounds:

1. Polymeric and dimeric lanthanide (Pr, Nd, Eu, Yb) compounds with amino acids, their phosphonic and hydroxamic analogues, and squaric acid. Cooperative effects and vibronic coupling, including the resonance effect, will be demonstrated through examination of spectra. Structural data and dynamics in solids will be considered on the basis of low temperature spectroscopy.
2. Lanthanide chelates, including mixed complexes of the $Ln\beta_3Ph$ type which are potential organic layered electroluminescent diodes. A number of important characteristic of these materials will be correlated with the donor–acceptor properties of the substituents in the ligands. For high symmetry $Ln(bpy\text{-}O_2)_4(ClO_4)_3$ chelates, circularly polarized luminescence (CPL) and total emission spectra will be analyzed and correlated with the racemization processes, and non-radiative quenching of the excited states.
3. Polynuclear lanthanide trichloroacetates and their heteronuclear Ln:Cu analogues. These are important as models for the investigation of magnetic exchange involving d and f electrons, and have potential applications in superconducting ceramics.

2. Cooperative interactions in lanthanide systems

In the spectra of lanthanides dimers or polymers containing Pr, Yb, Eu, and Nd four types of cooperative dimer transitions can be distinguished. These are listed below:

Type 1: Transitions to electronic dimer states.
Type 2: Simultaneous electronic and crystal field (CF) transitions on different metal centers.
Type 3: Simultaneous CF transitions on different metal centers within the ground electronic state.

*Tel.: +48-71-320-4300; fax: +48-71-328-2348.
E-mail address: jl@wchuwr.chem.uni.wroc.pl (J. Legendziewicz)

0925-8388/00/$ – see front matter
PII: S0925-8388(99)00735-5

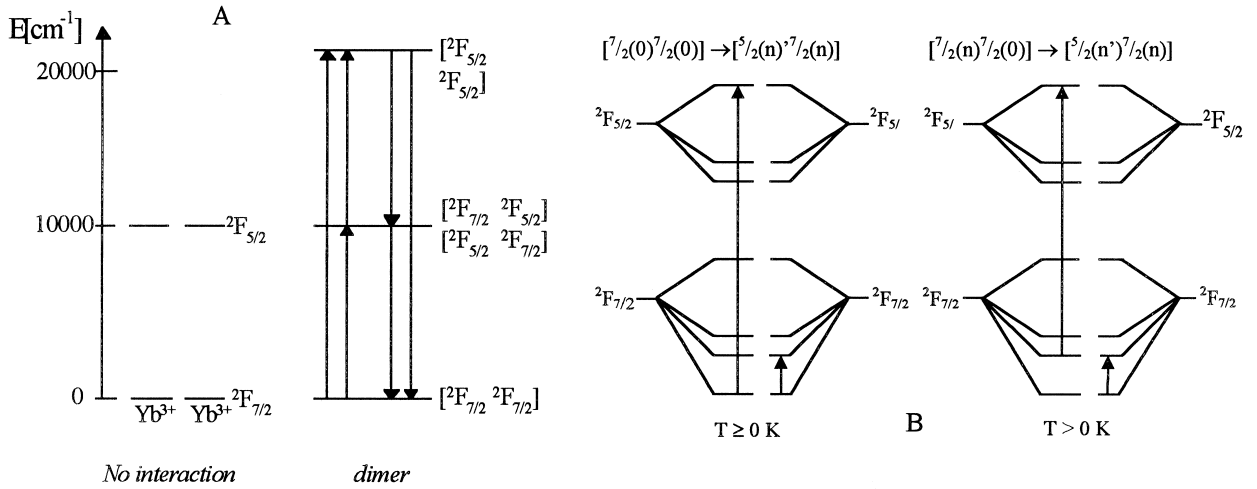

Fig. 1. (A) and (B): Schematic representation of singly and doubly excited states of Yb dimer. The arrows indicate the possible transitions for excitation and luminescence in the near infrared and visible spectral region.

Type 4: Transitions resulting from Heisenberg-type exchange interactions.

The first three types of transitions are accessible by optical spectroscopy and have been found in our systems [1–3]. They have also been reported by Güdel [4,5]. Type 1 and 2 transitions are depicted in Fig. 1A and B. Fig. 1A shows the doubly-excited dimer states for the cooperative interaction of two Yb(III) ions (5/2,5/2) at twice the energy of the $^2F_{7/2} \rightarrow {}^2F_{5/2}$ transition. These doubly excited dimer states are spectroscopically accessible from the ground state by one-photon or two-photon excitation processes. The second type of cooperative transition is presented in Fig. 1B. This example corresponds to the

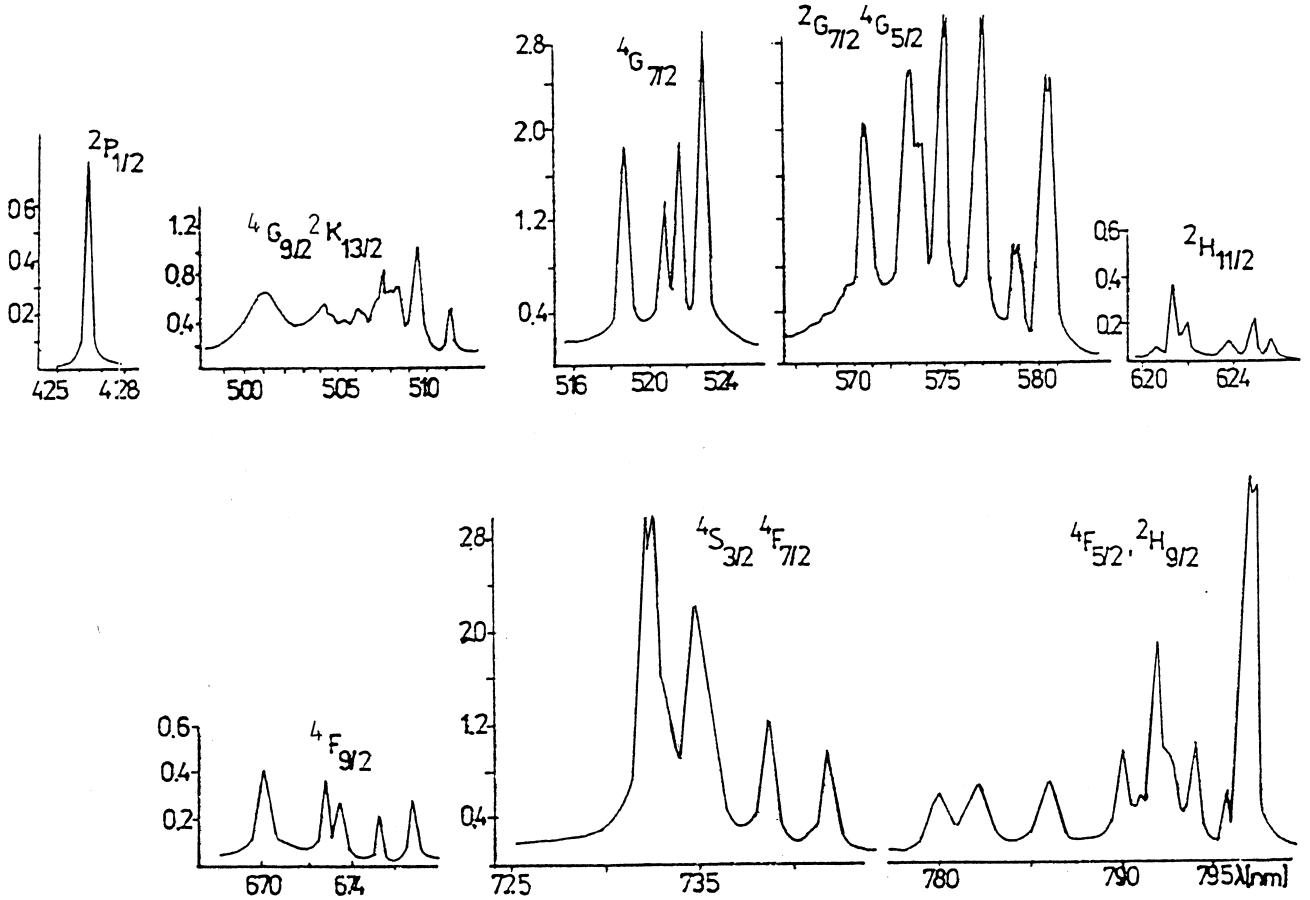

Fig. 2. Absorption spectrum of the $Nd(GlyGly)_2(ClO_4)_3 4H_2O$ single crystal at 5 K.

simultaneous electronic excitation of both Yb(III) ions by one photon. For [7/2 7/2]→[7/2 5/2] one of these excitations is between CF levels of the $^2F_{7/2}$ and $^2F_{5/2}$ terms, the other one involves a transition within the $^2F_{7/2}$ multiplet. In the third type of cooperative dimer excitation, CF components of the ground state multiplets ($^2F_{7/2}$,$^2F_{7/2}$) of both Yb(III) ions are active and a transition may be observed in the IR region.

The last type of dimer excitation can be observed by inelastic neutron scattering spectroscopy. In fact, further splitting of all the CF sublevels take place by exchange or magnetic multipole interactions, and then transitions between the split levels can be observed. This splitting usually does not exceed a few cm^{-1}. The exchange interaction leading to this splitting is of the Heisenberg type. We have found splitting of the order of a few wave numbers in the optical spectra of the polymeric lanthanide single crystals with diglycine (a) and in neodymium hydroxyperchlorates [2,6,7]. The X-ray structural data for (a) are presented in Figure 16b of Ref. [8], and Fig. 2 shows the corresponding absorption spectra in the range of the $^4I_{9/2}\rightarrow{}^4G_{5/2}$, $^2G_{7/2}$; $^4S_{3/2}$, $^4F_{7/2}$; $^4F_{5/2}$, $^2H_{9/2}$ transitions of the Nd(III) complex. The doublet structure of the bands seen in these spectra are a good illustration of this type of cooperative interaction.

Type 1 cooperative transitions have been detected in the spectra of polymeric Yb(III) trichloroacetate [9]. Inspection of the high energy region of the absorption spectra (see Fig. 3) at 482–484 nm shows several weak components detected only at low temperature. The intensity of the cooperative absorption is proportional to the square of the intensity of the fundamental $^2F_{7/2}\rightarrow{}^2F_{5/2}$ transition as expected. The calculated values for the oscillator strength for this system are as follows: 0.72×10^{-5} at 293 K; 0.56×10^{-5} at 4 K for the fundamental transition and $\approx1\times10^{-9}$ at 4 K for the cooperative absorption [9]. This result corresponds well to the theoretical calculation of cooperative absorption probabilities reported by Kaminski and Mironov [10].

The second type of cooperative interaction is frequently

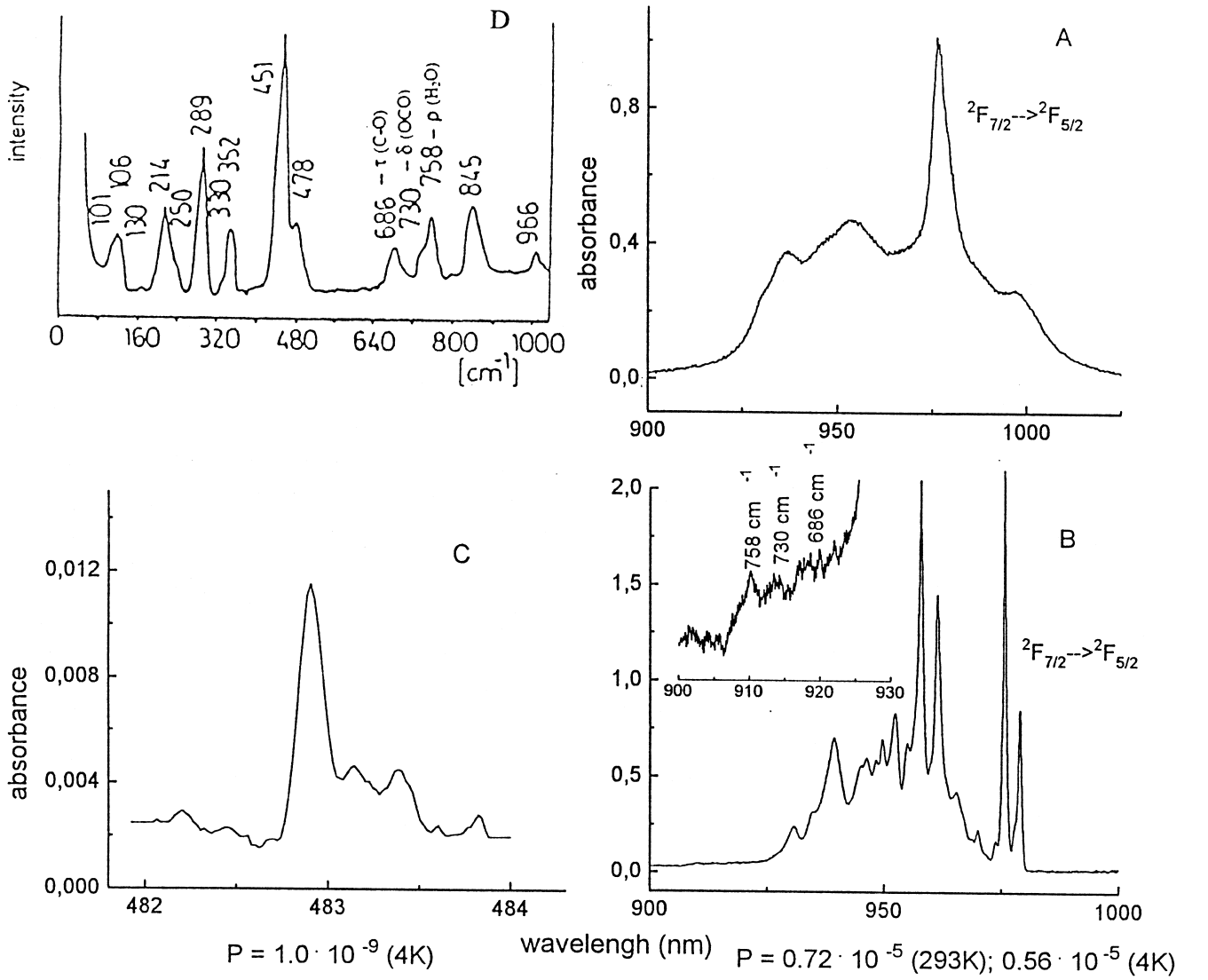

Fig. 3. Absorption spectra of $Yb(Cl_3CCOO)_3 2H_2O$ crystal at room (A) and 4 K (B) temperatures; (C) at 4 K; (D) Raman spectra at room temperature.

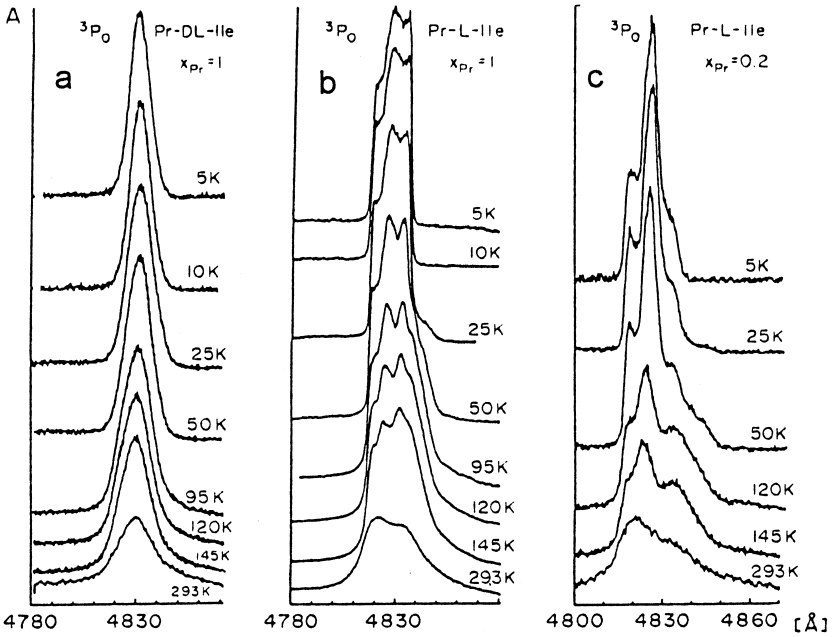

Fig. 4. Temperature dependence of $^3H_4 \rightarrow {}^3P_0$ transition in absorption spectra of the $[Pr(DL\text{-}Ile)_2(H_2O)_4]_2(ClO_4)_6$ (a), $[Pr(L\text{-}Ile)_2(H_2O)_4]_2(ClO_4)_6$ (b) and $[Pr_{0.2}La_{0.8}(L\text{-}Ile)_2(H_2O)_4]_2(ClO_4)_6$ (c).

observed in Yb^{3+} spectra (as mentioned above) and has also been seen in Pr^{3+} dimer systems with L and DL iso-leucine (Ile). In the structure of ytterbium trichloroacetate, metal ions reside in two non-equivalent structural position, thus in the $^2F_{7/2} \rightarrow {}^2F_{5/2}$ transition at 4 K, six components can be expected. In fact, three doublet components and a number of additional lines occur as a result of cooperative excitation of two ytterbium ions coupled in dimeric units. It is the case that, for this transition, some components can also be of vibronic origin (see Fig. 3). The next figure (Fig. 4) shows the results of cooperative excitation in the spectral range corresponding to the $^3H_4 \rightarrow {}^3P_0$ transition of praseodymium in centro- and noncentro-symmetric dimers of $[Pr(Ile)_2(H_2O)_4]_2(ClO_4)_6$ crystals. As can be seen in this figure, the number of lines observed exceeds that expected for two metal centers in the structure of $[Pr(L\text{-}Ile)_2(H_2O)_4]_2(ClO_4)_6$. As illustrated, dilution of this crystal leads to intensity changes for the lines associated with the cooperative interaction. Note that double excitation of pairs of ions leads to broadening of the bands in the centrosymmetric dimer (Fig. 4a), whereas in the noncentrosymmetric unit this results in the appearance of additional lines [11,12]. An explanation of these results is given in Fig. 5.

Cooperative effects may also be manifested in the nonlinear dependence of the f–f transition intensities on concentration of the active ions, as was demonstrated in the spectra of neodymium single crystals [11,12]. These results are given in Fig. 6 in which we show the dependence of calculated oscillator strength on concentration of Nd^{3+} ions in the range of 1–0.1 mol dm^{-3}.

In the spectra of polymeric squarate complexes with Eu(III), the cooperative transition involves the $^7F_1$ excited state of the Eu^{3+} ion; similar to the Eu_2O_3 system reported by Buys, Meijerink and Blasse [13]. The crystal structure for the two types of europium squarates: monomeric (1) and polymeric (2) have been previously published [14,15]. Their excitation spectra in the area of the $^7F_0 \rightarrow {}^5D_2$ transitions are plotted in Fig. 7 [2,16]. The intensities of the vibronic components in the region corresponding to internal ligand modes are comparable for the two types of monocrystals (monomeric and polymeric). However, significant differences are observed in the 0–400 cm^{-1} range from 0-phonon lines. This spectral range covers the energies associated with transitions due to cooperative interactions of pairs of ions coupled by the squarate ligand. The observed phenomenon could be caused by double excitation of pairs of europium ions mediated by phonons, whose energy corresponds to the splitting between the $^7F_0 - {}^7F_1$ levels.

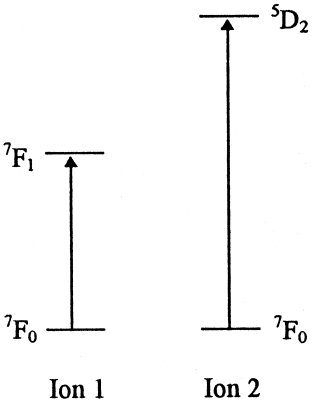

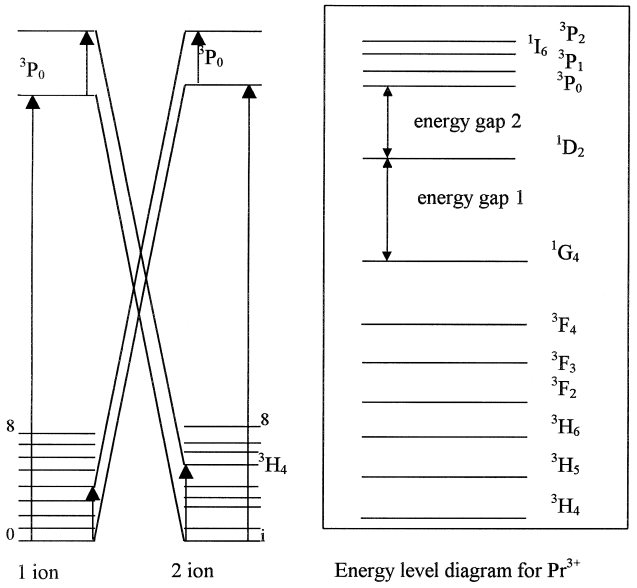

Fig. 5. The double excitation of a pair of Pr (III) ions in the chain. The resulting transition corresponds to the sum of the two single excitations, thus leading to a high energy side band of the $^3H_4 \rightarrow {}^3P_0$ electronic origin.

This could be explained in the following way: at 77 K, an electronic excitation of $^7F_0 \rightarrow {}^5D_2$ on one ion is coupled to $^7F_0 \rightarrow {}^7F_1$ excitation on a neighbouring Eu^{3+} ion in the chain. The resulting transition corresponds to the sum of the two single excitations, leading to a high-energy side band of the $^7F_0 \rightarrow {}^5D_2$ electronic origin. These can be denoted as $^7F_{0(1)} \rightarrow {}^5D_{2(1)} + {}^7F_{1(2)}$ (280 cm^{-1}) and $^7F_{0(2)} \rightarrow {}^5D_{2(2)} + {}^7F_{1(1)}$ (303 cm^{-1}). Phonons with energy of 280 and 320 cm^{-1} most probably mediate this process, fitting well the splitting of $^7F_1 - {}^7F_0$ levels [2]. Comparison of the electronic spectrum with Raman data allows the assignment of vibronic components at the high energy region of the 0-phonon lines [2,16].

We have also applied EPR to the study of these metal–metal interactions, especially in heteronuclear compounds. For example, Cu:Ln squarates and trichloroacetates have been synthesised. The EPR spectra for the $[Nd_2Cu(C_4O_4)_4(H_2O)_{16}]\cdot 2H_2O$, $CuNd_2(CCl_3COO)_8 \cdot 6H_2O$ compounds are presented in Figs. 8 and 9. Two types of signals are observed; those of the Nd(III) ions at low temperature (4.2–50 K), and one associated with Cu(II) at 100 and 300 K. Analysis of these spectra yields information concerning the Cu:Ln interaction with the coupling constants presented at the bottom of the figures [7,8]. Unexpectedly, in the EPR spectra of the $CuPr_2(CCl_3COO)_8 6H_2O$ crystal the Cu–Cu interaction were found to take place through the nonmagnetic Pr–Pr dimer unit. The mechanism of this interaction is still under investigation. [2,17–21].

Fig. 10a and b show results of an X-ray crystallographic analysis of the first known lanthanide compounds with amino-hydroxamic acids. The chirality of the ligand controls the composition of the complexes and the symmetry of the dimer units in the structure. Fig. 10a and b show views of the structures of europium compounds with DL (a) and L- (b) α-alanine-hydroxamic acids. In the chelation of the lanthanide ion, two oxygen atoms of the ligand molecule are involved; the NOH group plays a bridging role in the formation of the binuclear system. Both compounds consist of dimers in their structure. A centrosymmetric system exists in (a), whereas in compound (b) the dimer possess a C_2 axes. In addition a complex dynamic process occurs in the solids as a function of temperature. Analysis of the absorption, excitation, and emission spectra seems to confirm the centrosymmetric

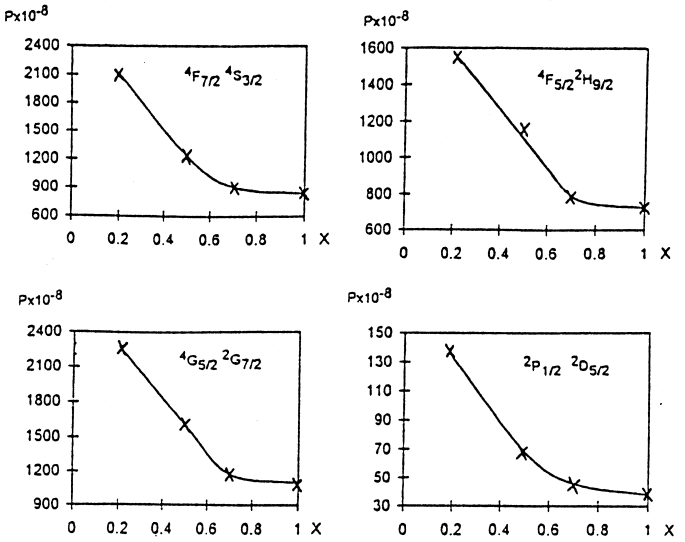

Fig. 6. The concentration dependence selected oscillator strength values of Nd (III) in the spectra of $[Nd_xLa_{1-x}(L\text{-Ile})_2(H_2O)_4]_2(ClO_4)_6$ compound.

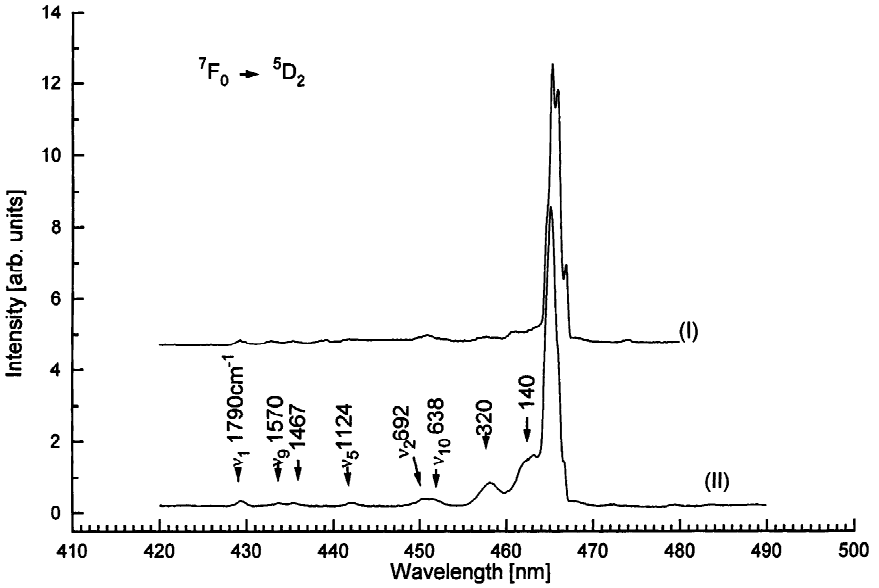

Fig. 7. Excitation spectra for compounds (I) and (II) in the region of $^7F_0 \rightarrow {}^5D_2$ transition; $T = 77$ K.

dimer structure of the europium racemic single crystal, at least in the 300–77 K temperature range (Fig. 11). However, upon lowering temperature to 4 K, a dynamic process occurs which can be explain by an intrasystem conformational change or phase transformation in the solid. At 77 K one component of the $^7F_0 \rightarrow {}^5D_0$ transition in the absorption spectrum of crystal (a) was recorded, further decrease of temperature down to 4 K splits this component to two lines with concomitant rearrangement of absorption intensities. A similar effect was observed in the $^7F_0 \rightarrow {}^5D_2$ transition. This phenomenon is accompanied by variation in electronic transition probabilities and decay times (see Tables 1 and 2). Significant enhancement of intensities is observed in the 80–90 K region, and extreme-

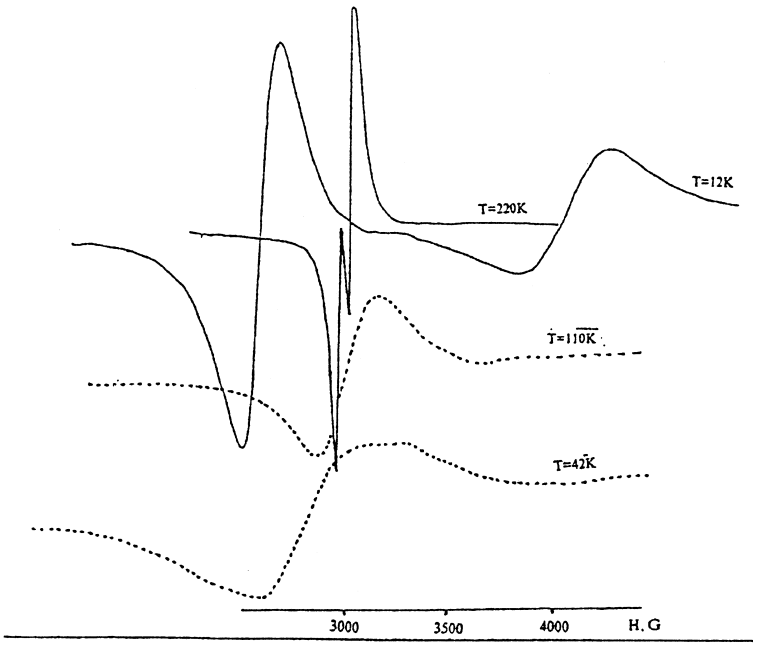

Fig. 8. The temperature dependence of the EPR spectra at an arbitrary orientation of the $[Nd_2Cu(C_4O_4)_4(H_2O)_{16}]2H_2O$ crystal. The EPR spectra were recorded at 9.3 GHz (X-band) in the temperature range from room to 10 K and at 4.2 K using an ERS-230 radiospectrometer. Single crystal spectra were recorded in three orthogonal planes. The linewidth of the HT signal increases as the temperature is lowered and at $T < 70$ K this signal is not practically detected. The LT spectra were detected at $T < 60$ K. The linewidth decreases and the intensity of the LT spectra increases as the temperature is lowered. $J^{Cu-Nd} = 0.2$ cm^{-1}.

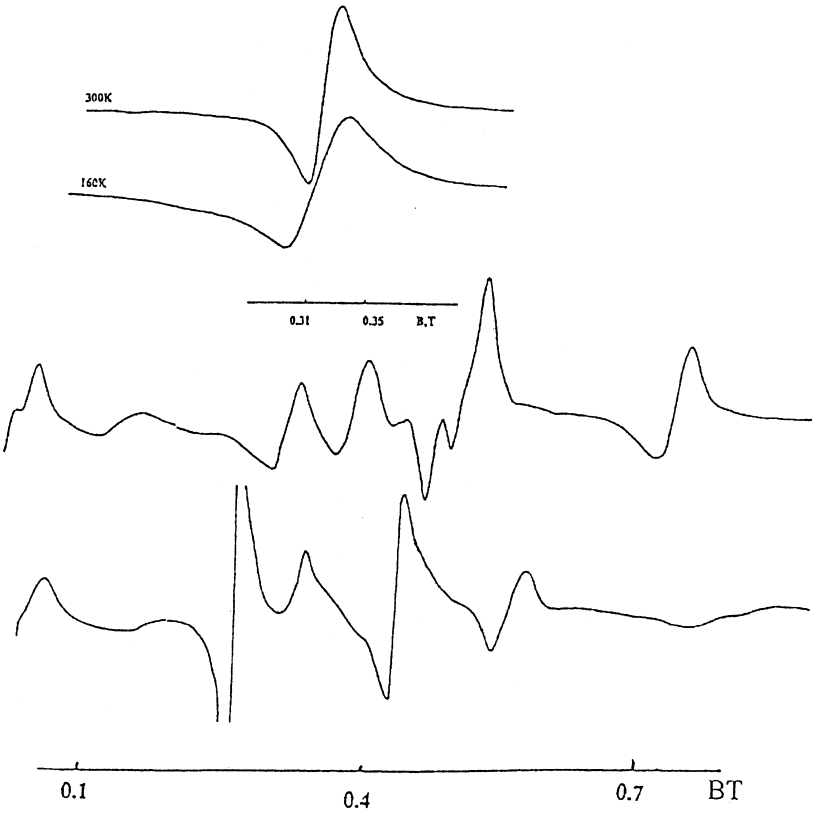

Fig. 9. The low temperature EPR spectra of $CuNd_2(CCl_3COO)_8 6H_2O$ crystal at $T=10$ K for two arbitrary orientations and at high temperature $J^{Cu-Nd}=0.9\ cm^{-1}$.

ly large changes are observed at 5 K for all the transitions recorded. Strong variations of decay times in the same temperature range as that observed in absorption spectra confirm the transformation of the structure. This dynamic process was found only in racemic systems and depends on the lanthanide ionic radius [22,23].

The two-dimensional polymeric structure of a europium complex with phosphono-methylglycine (Eu PMG) will now be discussed. This species has an unexpected architecture in which oxygen atoms of perchlorate anions are engaged in metal ion coordination in addition to coordination to the PMG groups The structure is given in Fig. 12. Two types of centrosymmetric dimeric units, created by carboxyl and phosphonic groups, are formed. In fact, this complex is only the second example of a lanthanide compound with innersphere perchlorate ion coordination in the series of amino-acids complexes. This result is good confirmation of the competition between water molecules and perchlorate anions in the coordination of metal ions in aqueous solutions. Electronic spectra also confirm the complex structure of this compound. The $^5D_0 \rightarrow {}^7F_0$ transition plotted in Fig. 13 shows the existence of two sites for the metal ion in the structure. Its shift can be treated as a nephelauxetic effect caused by carboxyl and phosphonic group coordination.

Vibronic components are compiled in Table 3, and the modes which promote vibronic transitions are mainly associated with those groups which are coordinated to the metal ion [24]. This is important in the studies of metal ion bonding in biological systems. The results are in good agreement with the theory of vibronic transition probabilities. According to the consideration of Blasse et al. this can be described as follows [25,26]:

$$P_v \approx \nu(g + n\alpha R^{-3})^2 \Xi(1,2)^2 \langle J \| U^{(2)} \| J' \rangle^2 [1/(2J+1)] \langle 0 \| T^{(1)} \| p \rangle^2 \quad (1)$$

where P_ν is the oscillator strength of the vibronic transition involved at frequency ν; n is the number of ligands around metal ion (M); g and α are, respectively, the charge and polarizability of the ligand; R is the M-ligand distance; the factor $\Xi(1,2)$ is defined by Judd [27], and is connected with the opposite-parity configuration mixing; and J and J' are the quantum numbers of the initial and final electronic states. $\langle \| U^{(2)} \| \rangle$ is the matrix element of the reduced tensor operator, and $\langle \| T^{(1)} \| \rangle$ is the matrix element of the operator connecting the (0) and (p) vibrational states. The last terms in this relation remain the same in the system under consideration. Thus, the intensities of the vibronic components can be related to the former ones and correspond to the strength of metal–ligand bonding, and charge and polarizability of the ligand.

Lanthanide chelates belong to the next group of compounds which is the subject of much research. They have

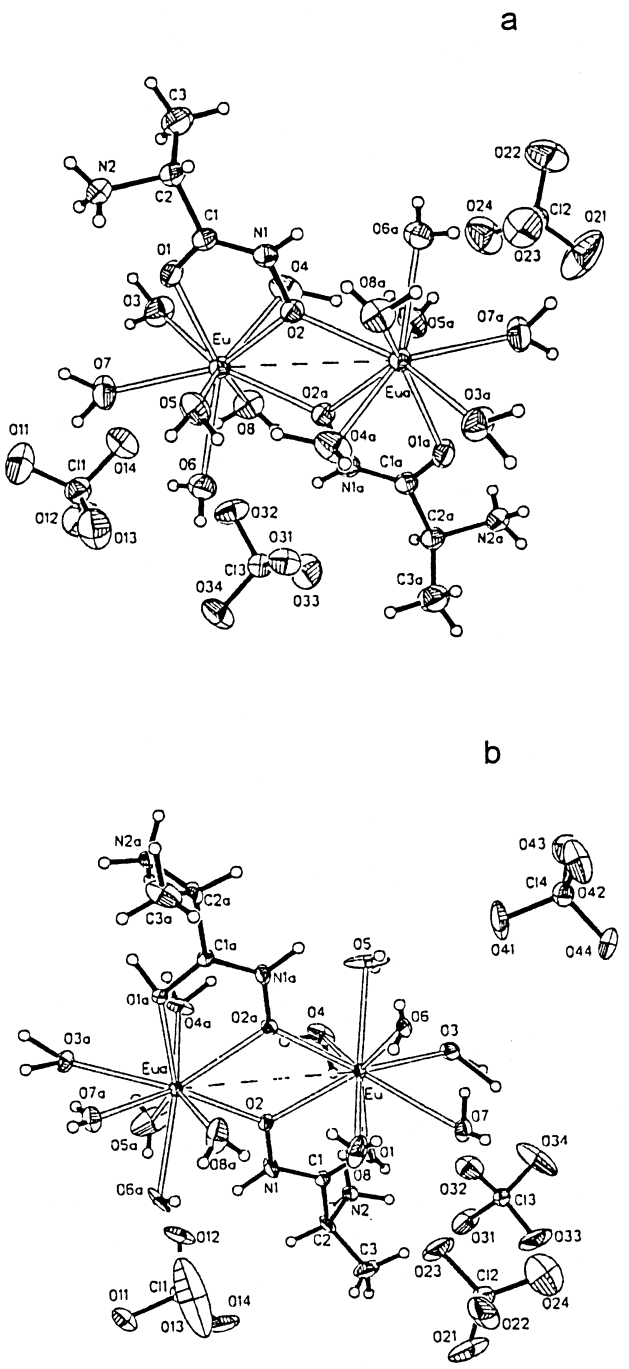

Fig. 10. Crystal structure of (a) [Eu(DL-α-Alaha)$(H_2O)_6]_2(ClO_4)_6$: space group $P2_1/n$, $a=10.347(1)$ Å, $b=11.289(2)$ Å, $c=16.968(3)$ Å, $\beta=95.39°$; Eu–Eua = 4.114 Å; (b) [Eu(L-α-AlahaH)$(H_2O)_6]_2(ClO_4)_8$: space group $C2$, $a=19.912(3)$ Å, $b=8.620(2)$ Å, $c=15.881(3)$ Å, $\beta=107.37(3)°$; Eu–Eua = 4.079 Å.

become increasingly important due to the expanding use of these type of compounds as MRI contrast agents, and as luminescence probes in biological systems. The interest in developing the spectra is also motivated by the application of lanthanides in solid-state magnetic and optical devices. A number of lanthanide mixed β-diketonates ($Ln\beta_3Ph$) compounds have been used recently in organic layered electroluminescent diodes; (OLEDs). A number of important characteristics of these materials affecting the intensity of electroluminescence, such as stability of compounds, mobility of the charge carriers, and height of the potential barriers for charge carrier injection, have been correlated with the donor–acceptor properties of the substituents of ligands [28,29]. Furthermore, these donor–acceptor properties influence the energy and intensity of the ligands and Ln^{3+} ions transitions in absorption and luminescence, vibrational states and electron–phonon interactions, and energy transfer and quantum yields of the luminescence of lanthanide β-diketonates. Analysis of the total spectral data permits the evaluation of the applicability of different β-diketonates in OLEDs.

Data for a series of europium β-diketonates are collected in Tables 4 and 5 together with Taft's constant of different radicals of β-diketone molecules. Acceptor properties of the substituents increase from dipivaloylmethane (DPM) $\Sigma\sigma^* = -0.8$ to hexafluoroacetyloacetone (HFAA) ($\Sigma\sigma^* = 5.2$). The phenanthroline derivatives are arranged with increasing acceptor properties of their radicals. It is important to point out the main factors describing the properties of these systems, namely, the nepheloauxetic effects (NE), and the crystal field parameters. These are both included in Table 5. The substituents with different D–A properties in the β-diketone molecules change the distribution of the π-electronic density in the chelating rings as well as effective charges on the oxygen atoms. This leads to the change of the contribution of covalency to the Ln–O bond, and to changes of the bond strengths and distances in the Ln–O and Ln–N cases. Similar effects are observed with variation of the substituents for the second kind of ligand (1,10-Phenanthroline). The degree of covalency of the metal–ligand bonds may be characterised by shifts of the $^5D_0 \rightarrow {}^7F_0$ transition in Eu^{3+} spectra. The variation of Eu–O and Eu–N bond properties due to nepheloauxetic shifts depends on the donor–acceptor properties of the substituents in both types of ligands. The most effective luminescence of Eu^{3+} is observed through ligand band excitations, where the ligand bands are in resonance with the $^7F_0 \rightarrow {}^5D_4$ (365 nm) and $^7F_0 \rightarrow {}^5G_6$ (375 nm) transitions of Eu^{3+}. In non-radiative quenching processes both the triplet states of the ligands and the CT states could contribute. The lowest quantum yield of europium luminescence in Eu(β_3)Nphen is due to quenching of $^5D_0$ excitation energy through the lowest triplet state of the Nphen moiety.

It is worth noting that the intensities of vibronic components increase with the increasing of covalency, thus confirming the theory of vibronic transition probabilities as it was described earlier. Moreover, in this case nonradiative deactivation promoted by this phonons is also more effective. Comparison of the CF parameters calculated for the systems presented here, and NE shows significant similarities of the two systems, Eu(DPM)Ph (3a, b) (1) and $Eu(TTF)_3Nphen$ (2) for which (with the exception of

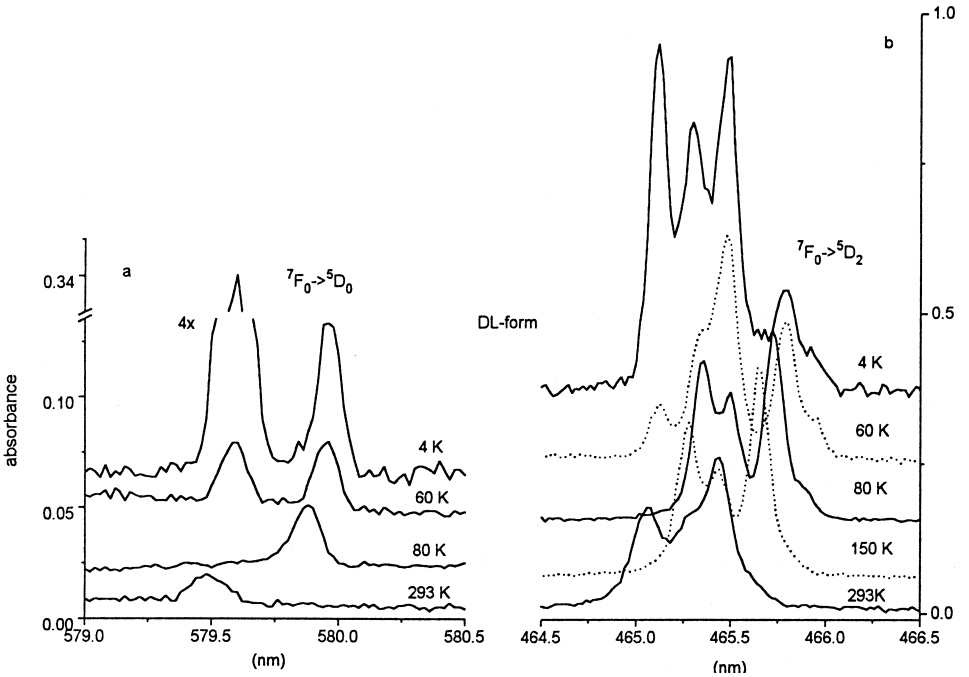

Fig. 11. Temperature dependence of $^7F_0 \rightarrow {}^5D_0$ and $^7F_0 \rightarrow {}^5D_2$ transitions in the spectra of [Eu(DL-α-Alaha)$(H_2O)_6]_2(ClO_4)_6$ crystal.

Table 1
The oscillator strength values of f–f transitions of the [Eu(DL-α-Alaha)$(H_2O)_6]_2(ClO_4)_6$ single crystal[a]

Term	$P_{exp} \times 10^8$				
	293 K	150 K	80 K	60 K	4 K
$^7F_0 \rightarrow {}^5D_0$	0.21	–	–	0.25 I 0.25 II	2.15 I 0.55 II
$^7F_0 \rightarrow {}^5D_1$	1.18	–	–	2.56	5.53
$^7F_1 \rightarrow {}^5D_1$	4.92	–	–	–	–
$^7F_0 \rightarrow {}^5D_2$	10.90	11.45	11.18	13.13	23.31

[a] $D_m = 2.11$ g/cm^3, $C_m = 3.78$, $l = 0.0567$ cm.

B_2^4) all other CF parameters are the same (Tables 4 and 5). So the effect of the acceptor properties of one ligand on the charge distribution of the coordinating atom of the second ligand is adequate to cause an increase in the donor properties of the second ligand. As a consequence this leads to comparable properties of compounds 1 and 11 in Table 5. That is, the intensities and distribution of vibronic components is similar (see Fig. 14) in the spectra of compound 1 and 11 consistent with the theory of vibronic transition probabilities (Eq. (1)). Taking into account the total spectral data one could suppose that fluorinated β-diketones Eu(TTFA)$_3$Ph and Eu(OTOFOD)$_3$Ph can be used in OLEDs.

Table 2
Decay times of [Eu(DL-α-Alaha)$(H_2O)_6]_2(ClO_4)_6$[a]

T (K)	223	173	85	77	60	40	14
τ (μs)	141.0	193.0	209.0	279.8	321.0	398.0	428.0

[a] For [Eu(L-α-AlahaH)$(H_2O)_6]_2(ClO_4)_8$ τ (μs) = 253.0 (77 K).

Let us focus on one more aspect of the electron–phonon coupling in chelate systems. If the energy of phonons remains in resonance with the splitting of the Stark components of the electronic transitions in emission, subtle splitting of components in the emission spectra appears. Additional lines in the emission can be observed, and changes in the vibronic component intensities also occurs. These effects first were reported by Caro [30] in 1985, and later observed by Richardson in the spectra of high symmetry europium antipyrine complexes [31]. We have found this phenomenon in the spectra of Eu(HMPA)$_6$(ClO$_4$)$_3$ crystals with O_h symmetry [32] in the spectra of phosphono- derivatives of β-diketones and in mixed Euβ$_3$Ph complexes [28,29,33]. Recently, Malta in his theoretical work, presented a theoretical description of this effect which correlates well with our experimental results [34].

The next figure shows the resonance effect in mixed complexes of Eu(Ac)$_3$Ph. The intensities of the respective vibronic and electronic components depends on the condition of resonance (see Fig. 15a, b and c) which can be effected by changes in the frequencies of vibrational modes in deuterated ligand molecules.

Previous studies of the crystal structure of La(III) compound formed with 2,2′-bipyridine-1,1′-dioxide (bpyO2) have shown the existence of an tetrakis eight coordinate complex in which the metal ions occupy sites of almost exact D_4 symmetry. The appearance of several crystal field transitions in the emission for the Eu(III) complex are interpreted in terms of distortions to D_2 from the D_4 symmetry seen for the La(III) analogue. Large circularly polarized luminescence is observed from

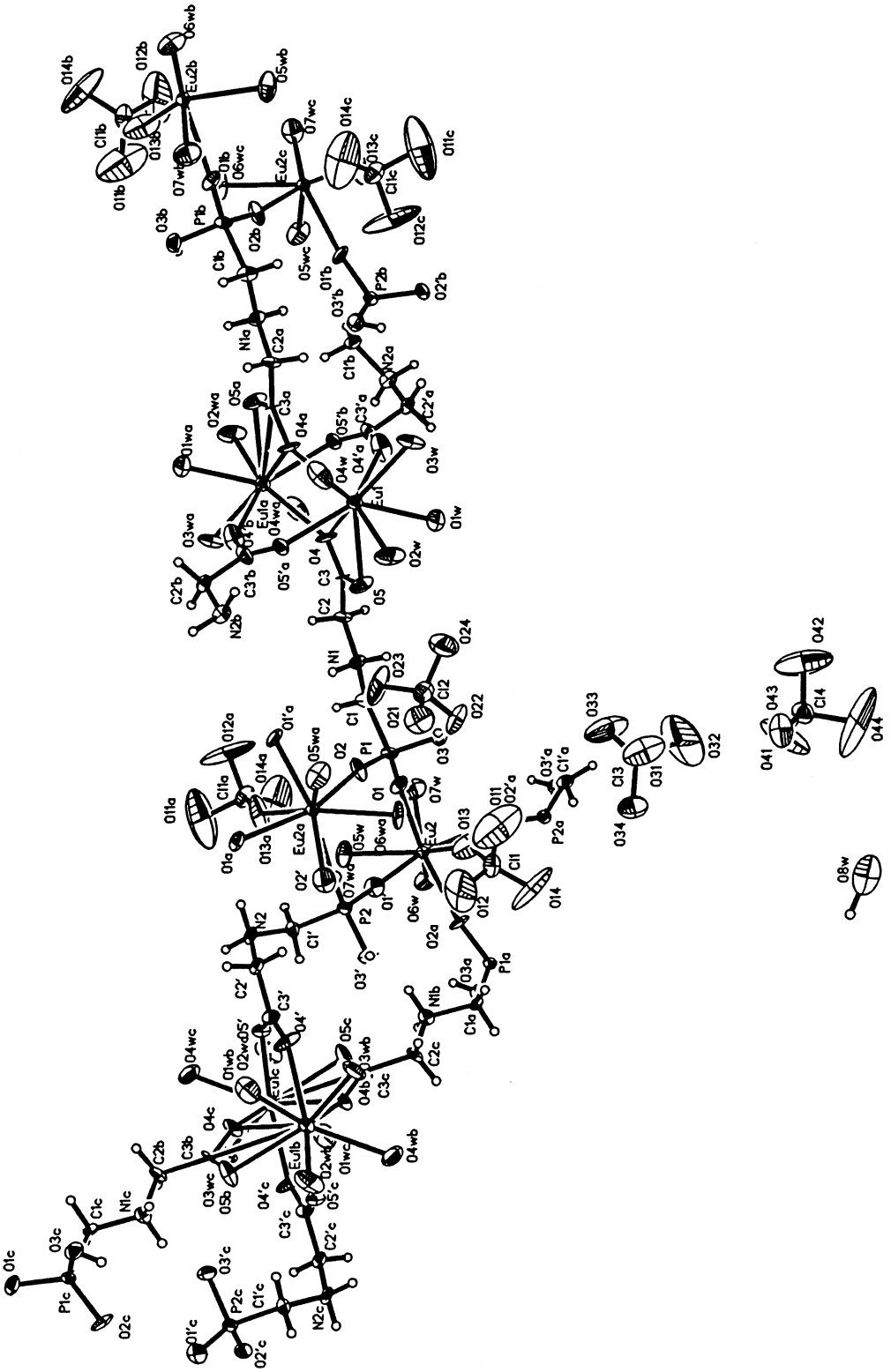

Fig. 12. Crystal structure of the $Eu_2(HO_3PCH_2NH_2CH_2COO)_2(H_2O)_8(ClO_4)_4$ complex.

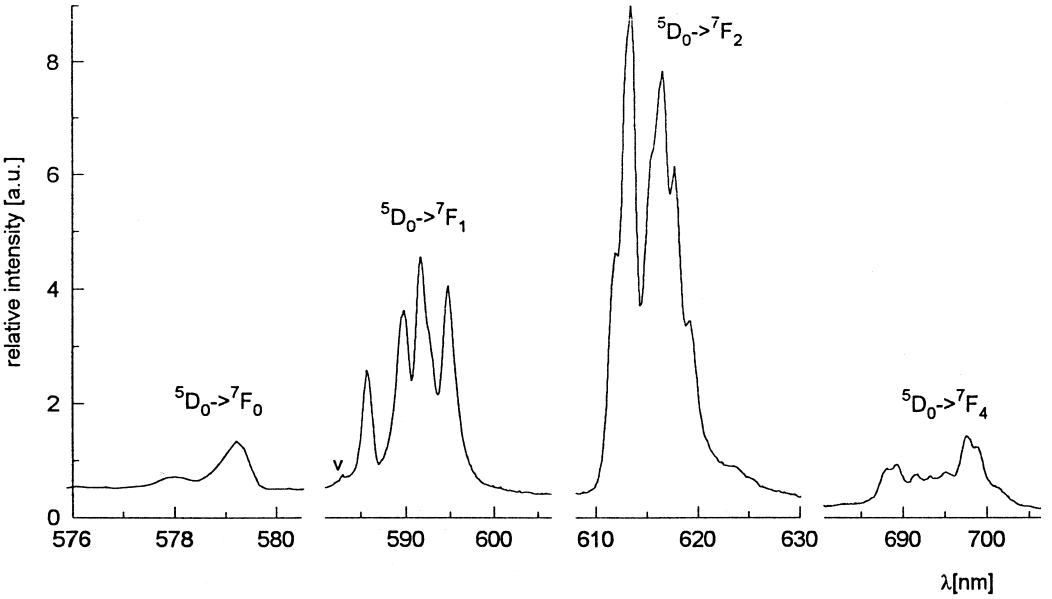

Fig. 13. Emission spectrum of the $Eu_2(HO_3PCH_2NH_2CH_2COO)_2(H_2O)_8(ClO_4)_4$ crystal at 77 K.

Table 3
Vibronic components in luminescence and excitation spectra of the $Eu_2(HO_3PCH_2NH_2CH_2COO)_2(H_2O)_8(ClO_4)_4$ crystal

Transition	Energy (cm^{-1})	ΔE (from 0-phonon line) (cm^{-1})
$^5D_0 \rightarrow {}^7F_2$	16,811	
	17,154	343 δ (COO)
$^7F_0 \rightarrow {}^5D_2$	21,505	
	21,633	128 δ (LnOLn)
	21,798	293 ν (LnO)
	22,067	562 π(COO)
	22,185	680 τ (OCO)
	22,585	1080 ν_s (ClO_4)
	22,655	1150 ν (PO)
	22,740	1232 ν (Cl–O_4)

$Eu(bpyO2)_4^{3+}$ in acetonitrile solution following circularly polarized laser excitation. This results suggests that the complex occurs in solutions as a racemic complex that does not racemise on the emission time scale, and also confirms (on the basis of the selection rule) the D_2 symmetry of the Eu(III) centre in solution. Extraordinarily large absorption and emission intensities for the hypersensitive transitions of $Nd(bpyO2)_4^{3+}$ and $Eu(bpyO2)_4^{3+}$ are observed, and can be explained only in the terms of the dynamic polarizability mechanism for transitions obeying the selection rule $\Delta J = 0 \pm 2$. For the $^4I_{9/2} - {}^4G_{5/2}$, $^2G_{7/2}$ transition of the Nd(III) complex in acetonitrile the calculated oscillator strength is 7900×10^{-8}, and for the $^7F_0 - {}^5D_2$ absorption in the Eu(III) complex the value is 100×10^{-8}. In D_4 and D_2 symmetry one must consider the anisotropic polarizability of the ligands in order to obtain the second -rank ligand tensor necessary for electric dipole intensity of the quadrupole ($\Delta J = 0 \pm 2$) transition.

Another interesting aspect of the spectroscopy of the Tb(III) compound was found. No emission is observed for Tb(III) by direct or indirect excitation (by ligand bands) in solution at room temperature. This result suggests the importance of energy ''back'' transfer from Tb(III) to the ligand orbitals. The emission of this compound in solution and the solid state is temperature dependent, and reflects details of the relative location of the ligand singlet and triplet levels relative to the Tb(III) energy levels. The mechanism of the competing excited states processes is the

Table 4
Taft's constants of different radicals of β-diketones (β-diketone = R_1–CO–CH_2–CO–R_2)

		R_1	R_2	σ^*_1	σ^*_2
1	DPM	–$C(CH_3)_3$	–$C(CH_3)_3$	−0.4	−0.4
2	AA	–CH_3	–CH_3	0	0
3	BA	–CH_3	–C_6H_5	0	+0.6
4	DBM	–C_6H_5	–C_6H_5	+0.6	+0.6
5	FOD	–$(CF_2)_2CF_3$	–$C(CH_3)_3$	+3.7	−0.4
6	TTFA	–CF_3	–C_4H_3S	+2.6	+1.35
7	GOFGD	–$(CF_2)_2OCF_3$	–C_6H_5	+3.7	+0.6
8	OTOFOD	–$CF_3(CF_2)_2OCF(CF_3)$	–C_6H_5		+0.6
9	HFAA	–CF_3	–CF_3	+2.6	+2.6

Table 5
Positions of $^5D_0$ level (cm^{-1}), crystal field parameters (cm^{-1}) and intensities of $^5D_0 \rightarrow {}^7F_2$ transition

Compound	$^5D_0 \rightarrow {}^7F_0$ 77 K	B_0^2	B_2^2	B_0^4	B_2^4	B_4^4	I_{0-2}/I_{0-1}	
		CFP, 77 K					77 K	300 K
$Eu(DPM)_3 \cdot Phen$	17,241	705	87	−1605	−536	733	12.1	9.2
$Eu(AA)_3 \cdot Tmphen$	17,221	580	122	−1424	−466	758	8.2	9.7
$Eu(AA)_3 \cdot Phen$	17,247	653	188	−1413	−530	772	7.8	7.0
$Eu(BA)_3 \cdot Phen$	17,256	596	175	−1603	−594	671		
$Eu(FOD)_3 \cdot Tmphen$	17,209	425	105	−1519	−578	520	12.0	
$Eu(FOD)_3 \cdot Phen$	17,238	472	198	−1547	−530	590	11.9	13.2
$Eu(FOD)_3 \cdot Dphphen$	17,212	490	221	−1615	−531	573	12.2	
$Eu(FOD)_3 \cdot Nphen$	17,209	553	139	−1571	−515	737	12.0	
$Eu(TTFA)_3 \cdot Tmphen$	17,235	345	180	−1636	−565	537	13.9	16.3
$Eu(TTFA)_3 \cdot Phen$	17,244	622	116	−1580	−629	759	10.2	11.4
$Eu(TTFA)_3 \cdot Nphen$	17,241	635	87	−1606	−615	726	12.6	12.4
$Eu(GOFGD)_3 \cdot Phen$	17,230	518	94	−1659	−678	541	12.3	13.8
$Eu(OTOFOD)_3 \cdot Phen$	17,221	520	105	−1751	−579	608	11.8	13.8

subject of on-going high-pressure studies as well as in spectroscopy in sol–gel matrices [35,36].

The last class of compounds to be discussed here is heteronuclear Ln:Cu trichloroacetates. A series of isomorphic single crystals from Pr(III) to Gd(III) have been obtained. The X-ray diffraction, magnetic and spectroscopic studies were undertaken in the range 300–1.7 K, and results have been related to the polynuclear lanthanide trichloroacetates [37–40]. The crystal structure of the $CuLn_2(CCl_3COO)_8 6H_2O$ compounds consist of heteronuclear chains composed of noncentrosymmetric dimers of two Ln_9 and Ln_8 polyhedra, bridged by three bidentate carboxylic groups and one chelating bridging type. These dimeric units are further linked by Cu_4 planar squares connected with Pr(III) ions by carboxyl groups and two water molecules, therefore forming strongly distorted octahedron of copper ions. The intrachain distances important for M–M interactions, are as follows: Pr1–Pr2 = 4.59 Å; Cu1–Pr1 = 4.345 Å; Cu1–Pr2 = 4.157 Å, whereas the interchain separation is equal to ~9.47 Å between Pr1

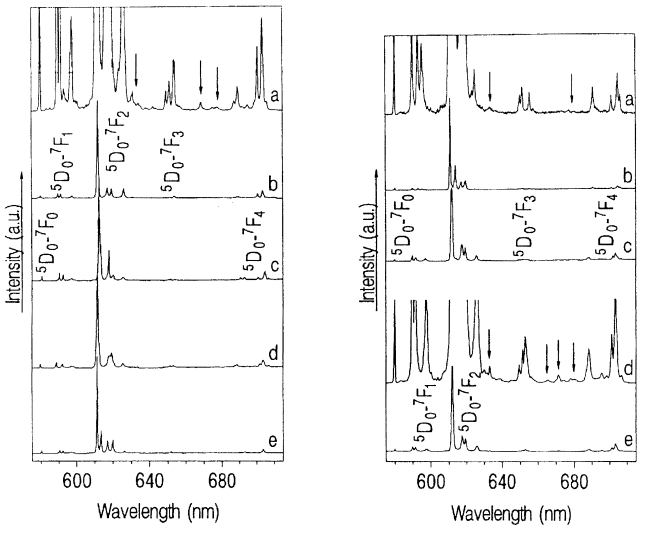

Fig. 14. (a) Luminescence spectra of $Eu(DPM)_3Phen$ (a, b), $Eu(AA)_3Tmphen$ (c), $Eu(AA)_3Phen$ (d) and $Eu(OTOFOD)_3Phen$ (e) at 77 K. (b) Luminescence spectra of $Eu(TTFA)_3Tmphen$ (a,b), $Eu(TTFA)_3Phen$ (c) and $Eu(TTFA)_3Nphen$ (d, e) at 77 K. Vibronic satellites are marked by arrows.

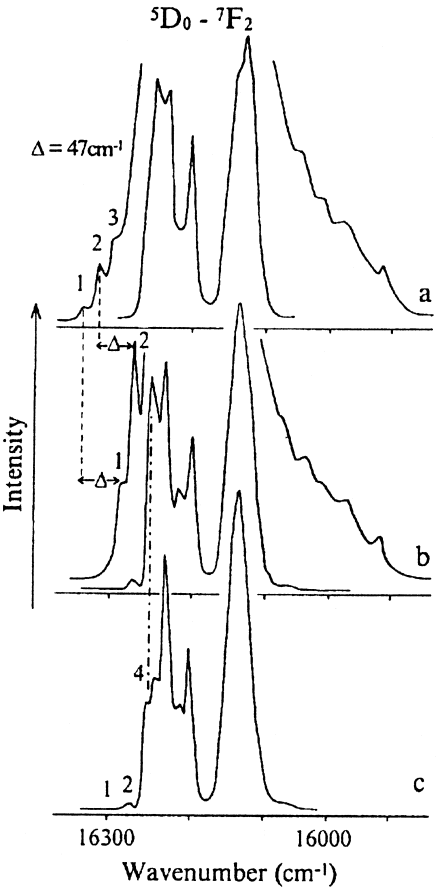

Fig. 15. Luminescence spectra of $Eu(CD_3COO)_3Bpy$ (a), $Eu(CH_3COO)_3Bpy$ (b) and $Eu(CH_3COO)_3D$-Bpy (c) in the region of $^5D_0 \rightarrow {}^7F_2$ transition at 77 K.

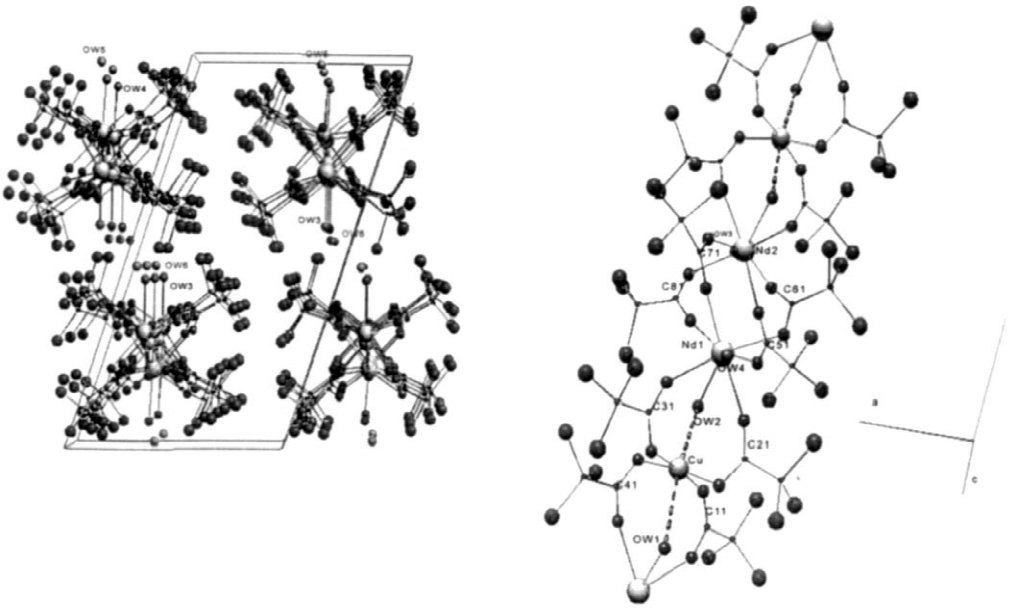

Fig. 16. View of the structure of $CuNd_2(CCl_3COO)_8 6H_2O$ monocrystal; Nd(1)–Nd(2)=4.3 Å; Cu–Nd(1)=4.1 Å; Cu–Nd(2)=4.14 Å; interchain Nd(1)–Nd(2)=9.47 Å and Cu(1a)–Cu(2b)=8.78 Å.

and Pr2, and ~8.78 Å between Cu1a and Cu2b (see Fig. 16).

The complex structure of these systems is well manifested in optical and magnetic data. The absorption spectrum of a heteronuclear crystal at 4 K is presented in Fig. 17. The broad d–d band of Cu(II) at 692.62 nm splits into two components (651.04 and 808.42 nm) upon decreasing the temperature to 4 K. Two sites of the Ln(III) ions in noncentrosymmetric units are well manifested in the $^3H_4$–$^3P_0$ transition. Moreover, under these conditions the $^3H_4$–$^1G_4$ transition is easily detected, most probably strengthened by the Cu(II) d–d transition. Calculations of the electron transition probabilities both for the f–f and d–d transitions were performed and values of oscillator strengths are collected in Table 6. These values were used to evaluate the Judd–Ofelt parameters [27,41]. Unexpectedly, for both systems (polynuclear and heteronuclear) positive values were found for one set of the data, even with the relatively low error of estimation. A decrease of temperature to 4 K is accompanied by a decrease in most of the f–f transitions intensities, and a more pronounced decrease was detected for the d–d band. The strong temperature dependence of intensities could the results from strong vibronic coupling and CF effects. However, the low temperature electronic spectrum of the crystal revealed no vibrational fine structure in the d–d band. This kind of structure could be observed in the spin allowed d–d transitions of centrosymmetric metal complexes as

Table 6
The $\tau\times10^9$ parameters calculated at room temperature and the oscillator strength values of $Pr(Cl_3CCOO)_3\cdot2H_2O$ and $CuPr_2(Cl_3CCOO)_8\cdot6H_2O$ crystals at different orientations (1,2) and temperatures

$P\times10^8$	$Pr(Cl_3CCOO)_3\cdot2H_2O$		$CuPr_2(Cl_3CCOO)_8\cdot6H_2O$		
	293 K	4 K	1	2	
			293 K	293 K	4 K
$^3H_4\rightarrow{}^3P_2$	1828.87	1725.50	1786.50	1780.60	
$^3H_4\rightarrow{}^3P_1,{}^1I_6$	556.69	506.45	704.63	737.73	743.70
$^3H_4\rightarrow{}^3P_0$	240.45	157.43	282.27	235.10	100.46
$^3H_4\rightarrow{}^1D_2$	320.80	463.49	325.04	406.44	752.87
$^3H_4\rightarrow{}^1G_4$					90.32
$^3H_4\rightarrow{}^3F_3,{}^3F_4$	1534.99		1631.55	1632.64	649.01
$^3H_4\rightarrow{}^3F_2$	859.39		769.69	753.87	433.73
d–d Cu^{2+}			42,164.60	25,704.62	22,164.65
$\tau_2\times10^9$	13.30±5.58		8.69±5.02		
$\tau_4\times10^9$	5.11±2.40		7.48±2.16		
$\tau_6\times10^9$	50.78±4.38		49.37±3.97		

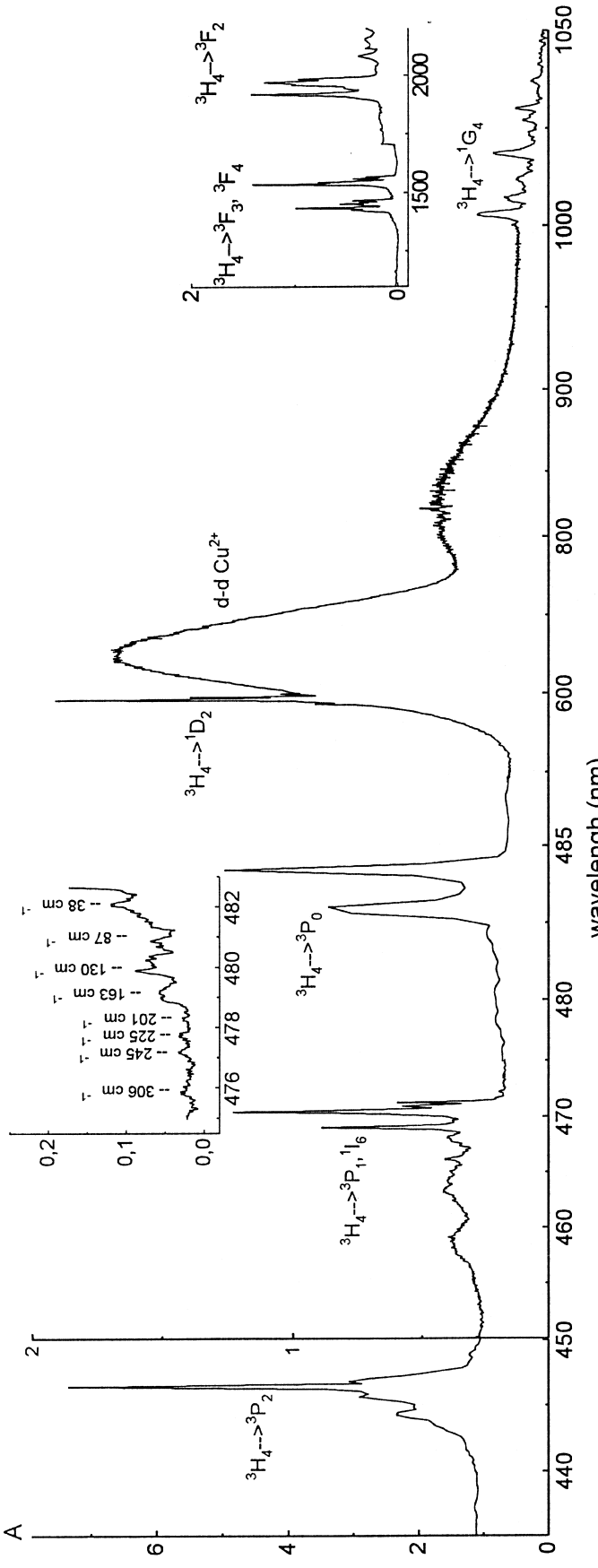

Fig. 17. Absorption spectrum of $CuPr_2(Cl_3CCOO)_8 6H_2O$ crystal at 4 K.

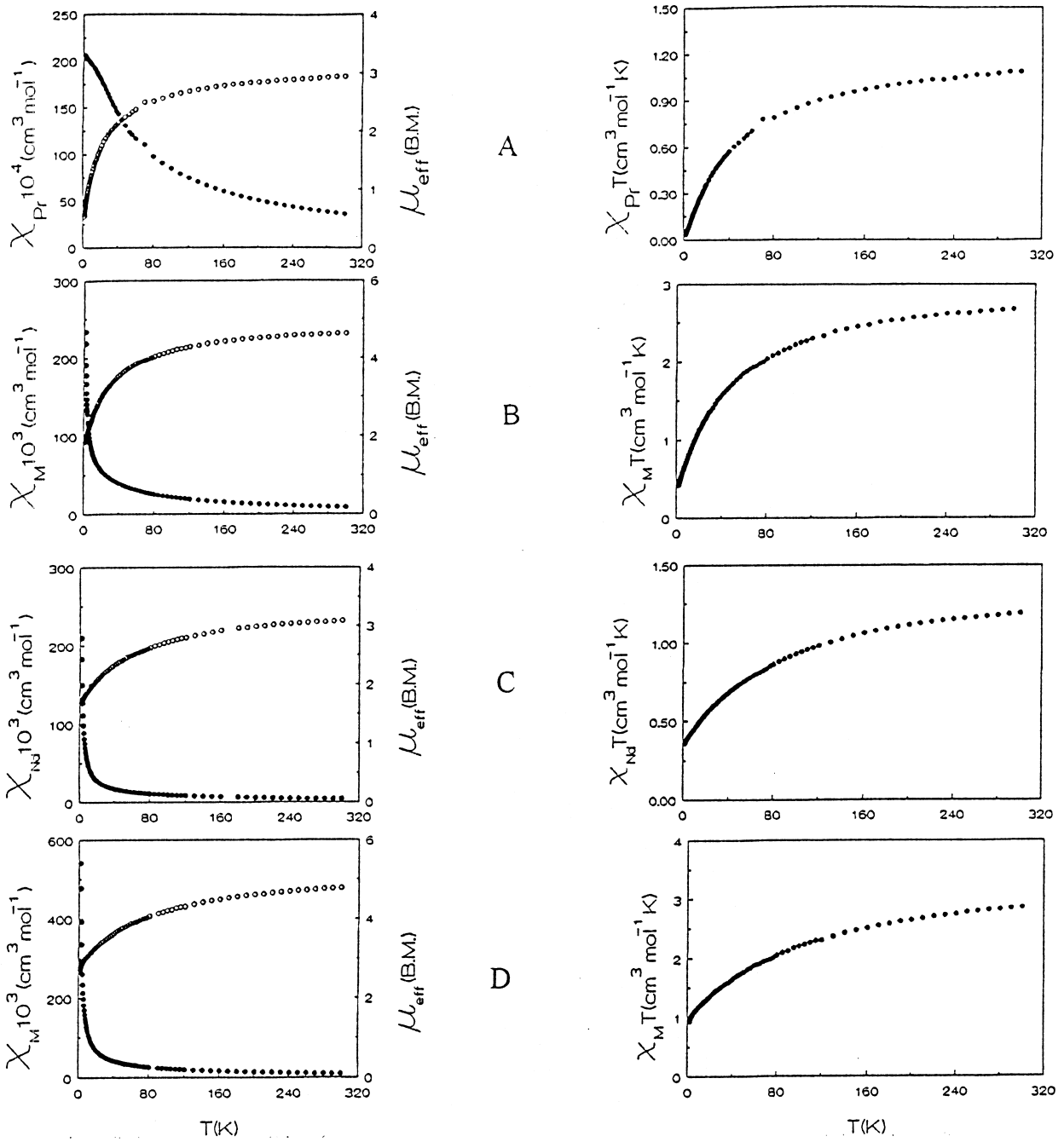

Fig. 18. Experimental magnetic data plotted as magnetic susceptibility χ (●), magnetic moment μ_{eff} (○) and χ. T calculated per molecule of complex: (A) $Pr(Cl_3CCOO)_3 2H_2O$, (B) $CuPr_2(Cl_3CCOO)_8 6H_2O$, (C) $NdCl_3CCOO)_3 2H_2O$, (D) $CuNd_2(Cl_3CCOO)_8 6H_2O$ vs. temperature.

several ungerade vibrational modes are available for inducing intensity. In fact, the overlapping the peaks produce a smooth structureless band [42].

The strong anisotropy of intensities confirm the distortion of the O_h symmetry in Cu coordination, and the Jahn–Teller effect is seen at low temperature. The low temperature spectra allow the determination of the energy level diagram, which can help in the consideration of magnetic properties. Experimental magnetic data plotted as magnetic susceptibility, χ_M and magnetic moments $\mu_{eff,}$ versus temperature are presented in next Fig. 18 and listed in Table 7 for a series of polynuclear compounds, and also for some heteronuclear systems. M–M interactions lead to the antiferromagnetic ordering, both in the heteronuclear Ln–Cu and the polynuclear Ln–Ln systems, with the exception of dysprosium trichloroacetate and $CuGd_2(CCl_3COO)_8 6H_2O$. The magnetic susceptibility changes with temperature according to the Curie–Weiss law with θ equal to -27.2 K for the Cu–Pr system and -54.1 for Cu–Nd. These results confirm the presence of

Table 7
The magnetic data of $CuPr_2(Cl_3CCOO)_8 \cdot 6H_2O$ (I) and $CuNd_2(Cl_3CCOO)_8 \cdot 6H_2O$ (II)

Temperature (K)	$\chi_M \times 10^3$ (cm^3 mol^{-1})		μ_{eff} [B.M.]	
	I	II	I	II
1.83	234	542	1.85	2.73
4.0	132	261	2.06	2.89
19.0	57.6	70.2	2.96	3.27
30.0	45.7	50.3	3.31	3.48
50.0	34.7	35.4	3.73	3.77
100.2	21.8	22.0	4.18	4.20
150.3	16.1	16.4	4.40	4.45
220.3	11.7	12.2	4.54	4.65
300.2	8.93	9.51	4.63	4.78

weak antiferromagnetic exchange coupling between the metal ions. The observed decrease of the magnetic moment with decreasing temperature may also be due to crystal-field effects. An almost non-magnetic state is created in the polynuclear Pr chloroacetate at 1.7 K. Our EPR investigations of the heteronuclear systems seem to confirm the presence of stronger Cu–Nd interaction than the Nd–Nd one, and weak Cu–Cu coupling in the Pr–Cu compound. A number of interesting results have been obtained in our laboratory from analysis of EPR spectra for systems such as these [17–21].

EPR investigations of the $CuNd_2(CCl_3COO)_8 6H_2O$ crystal show the presence of spin–spin interaction between Cu and Nd ions, and as consequence a complicated EPR spectrum is obtained. Analysis of the angular dependence of the EPR spectra allows to estimate the values of the isotropic exchange ($J_{ij}S_iS_j$) and the anisotropy of the Cu–Nd interaction ($S_i\{D_{ij}\}S_j$) for the three-nuclear Nd_1–Cu–Nd_2 fragment: $J_{Cu-Nd} = 0.9$ cm^{-1} and $D_{ZZ} = 0.2$–0.4 cm^{-1}. It has also been established that the interaction inside the fragments exceeds the interaction between them. This conclusion means that the interaction between the Cu and Nd ions exceeds the Nd–Nd interaction. It should be noted that the latter interaction is weaker than the isotropic spin–spin interaction and also the anisotropy parameters associated with the Cu–Nd interaction. The value of the isotropic part of the spin–spin interaction is estimated to be 0.9 cm^{-1}, and it is shown that this value and the anisotropy parameter of this interaction have comparable orders of magnitude (Fig. 9). Broadening of the spectrum of $CuNd_2(CCl_3COO)_8 6H_2O$ at room temperature indicates an increase of the ratio between the exchange interaction and the rates of the paramagnetic relaxation of the Nd ions, in comparison to that in the squarate crystal [17,18]. In the chain with the Pr(III) ions, correlation between the next nearest neighbouring spins is detected: a small interaction between Cu ions separated by dimeric subunits of the two rare earth ions is also observed. The magnitude of observed exchange is comparable to the hyperfine interaction, and depends on the temperature. It is proposed that at low temperature, when the ground state of the Pr(III) ion is nonmagnetic, the Cu spins are weakly coupled through the diamagnetic rare earth ions.

Acknowledgements

The author gratefully acknowledge the financial support of Polish Committee for Scientific Research (KBN) and National Science Foundation of USA for partial support of this work.

References

[1] J. Legendziewicz, J. Appl. Spectr. 62 (N4) (1995) 189.
[2] J. Legendziewicz, Acta Physica Polonica 90 (1) (1996) 127.
[3] J. Legendziewicz, in: W. Strêk, W. Ryba-Romanowski, J. Legendziewicz, B. Jeżowska-Trzebiatowska (Eds.), Excited States of Transition Elements, World Scientific Publishing Co. Pte. Ltd, Singapore, 1992, p. 149.
[4] M.P. Hehlen, H. Reisen, H.U. Güdel, Inorg. Chem. 30 (1991) 2273.
[5] M.P. Hehlen, H.U. Güdel, J. Chem. Phys. 98 (1993) 1768.
[6] E. Huskowska, J. Legendziewicz, Polyhedron 12 (1993) 2387.
[7] E. Huskowska, J. Legendziewicz, J. Hanuza, Polyhedron 9 (1990) 659.
[8] J. Legendziewicz, E. Huskowska, in: B. Jeżowska-Trzebiatowska, J. Legendziewicz, W. Stręk (Eds.), Excited States of Transition Elements, World Scientific Publishing Co. Pte. Ltd, Singapore, 1989, p. 228.
[9] J. Legendziewicz, M. Borzechowska, G. Oczko, J. Mroziñski, Spectrochim. Acta 54A (1998) 2197.
[10] V.S. Mironov, A.A. Kaminskii, Abstract of XXI RE Research Conference Duluth, USA, 1996, p. 89.
[11] J. Legendziewicz, Z. Ciunik, P. Gawryszewska, J. Sokolnicki, J. Alloys Comp. 225 (1995) 372.
[12] J. Legendziewicz, Z. Ciunik, P. Gawryszewska, J. Sokolnicki, Polyhedron 18 (1999) 2701.
[13] M. Buys, A. Meijerink, G. Blasse, J. Lumin. 37 (1987) 8.
[14] J.F. Petit, A. Gleizes, J.C. Trombe, Inorg. Chim. Acta 167 (1990) 51.
[15] E. Huskowska, T. Głowiak, J. Legendziewicz, G. Oremek, J. Alloys Comp. 179 (1992) 13.
[16] E. Huskowska, J. Legendziewicz, P. Drożdżewski, Acta Phys. Pol. A 90 (1996) 447.
[17] V.K. Voronkova, E. Huskowska, J. Legendziewicz, Yu.V. Yablokov, Solid State Physics 39 (1997) 2057.
[18] K.M. Salikhov, R.T. Galeev, V.K. Voronkova, Yu.V. Yablokov, J. Legendziewicz, Appl. Magn. Reson. 14 (1998) 457–472.
[19] V.K. Voronkova, J. Legendziewicz, G. Oczko, Yu.V. Yablokov, in: Proceedings of Third European ESR Meeting, Leipzig, Germany, 1997, p. 128.
[20] Yu.V. Yablokov, V.K. Voronkova, J. Legendziewicz, M. Borzechowska, Solid State Physics 41 (1999) 2154.
[21] V.K. Voronkova, Yu.V. Yablokov, G. Oczko, J. Legendziewicz, M. Borzechowska, New J. Chem., in press.
[22] J. Legendziewicz, P. Gawryszewska, E. Gałdecka, Z. Gałdecki, J. Lumin. 72–74 (1997) 559.
[23] E. Gałdecka, Z. Gałdecki, P. Gawryszewska, J. Legendziewicz, New J. Chem. 22 (1998) 941.
[24] J. Legendziewicz, P. Gawryszewska, E. Gałdecka, Z. Gałdecki, J. Alloys Comp. 275–277 (1998) 356.
[25] G. Blasse, Inorg. Chim. Acta 167 (1990) 33.
[26] G. Blasse, Int. Rev. Phys. Chem. 11 (1992) 71.
[27] B.R. Judd, Phys. Rev. 127 (1962) 750.

[28] V. Tsaryuk, V. Zolin, J. Legendziewicz, Spectrochim. Acta A 54 (1998) 2247.
[29] V. Tsaryuk, J. Legendziewicz, V. Zolin, L. Puntus, J. Sokolnicki, Proceeding of 9th CIMTEC, World Forum on New Materials: Advances in Science and Technology, 27, P. Vincenzini (Ed.), Techna Srl Faenza, Italy, 1999, pp. 299–306.
[30] P. Caro, O.K. Moune, E. Antic-Fidancev, M. Lemaitre-Blaise, J. Less Comm. Metals 112 (1985) 153.
[31] M.T. Berry, A.F. Kirby, F.S. Richardson, Mol. Phys. 66 (1989) 723.
[32] E. Gałdecka, Z. Gałdecki, E. Huskowska, V. Amirkhanov, J. Legendziewicz, J. Alloys Comp. 257 (1997) 182–190.
[33] V. Amirkhanov, C. Jañczak, L. Macalik, J. Hanuza, J. Legendziewicz, J. Appl. Spectr. (Russ) 62 (1995) 5.
[34] O.L. Malta, J. Phys. Chem. Solids 56 (1995) 1053.
[35] E. Huskowska, J. Legendziewicz, J.P. Riehl, (paper in preparation).
[36] E. Huskowska, J.P. Riehl, J. Lumin, in press.
[37] G. Oczko, J. Legendziewicz, J. Mroziñski, G. Meyer, J. Alloys Comp. 275–277 (1998) 219.
[38] J. Legendziewicz, M. Borzechowska, G. Oczko, J. Mroziñski, Spectrochim. Acta A 54 (1998) 2197.
[39] J. Legendziewicz, M. Borzechowska, G. Oczko, G. Meyer, New J. Chem. 24 (2000) 53.
[40] I. Kutlu, G. Meyer, G. Oczko, J. Legendziewicz, Eur. J. Solid State Inorg. Chem. 34 (1997) 231.
[41] G.S. Ofelt, J. Chem. Phys. 37 (1962) 511.
[42] C.D. Flint, Coord. Chem. Rev. 14 (1974) 47.